

## Article

# The Corrosion Behavior of Different Silver Plating Layers as Electrical Contact Materials in Sulfur-Containing Environments

Bingkun Yang<sup>1</sup>, Yun Chen<sup>1,\*</sup>, Wenkui Hao<sup>1</sup>, Yu Han<sup>1</sup>, Qiang Zhang<sup>1</sup>, Yujie Li<sup>2</sup>, Xiaofang Wang<sup>1</sup>, Luyao Huang<sup>1</sup> and Yiliang Lu<sup>1</sup>

<sup>1</sup> State Key Laboratory of Advanced Power Transmission Technology, State Grid Smart Grid Research Institute Co., Ltd., Beijing 102209, China; ybk\_511@163.com (B.Y.); hwk198516@163.com (W.H.); hany2003@126.com (Y.H.); zhangqianghgd@126.com (Q.Z.); misswangxiaofang@163.com (X.W.); hly\_0531@163.com (L.H.); yiliang\_lu@163.com (Y.L.)

<sup>2</sup> State Grid Jiangsu Electric Power Co., Ltd., Electric Power Science Research Institute, Nanjing 210000, China; liyufen915@126.com

\* Correspondence: helenchen9@163.com

**Abstract:** Isolation switching devices are vital components in power grids. During their operational lifespan, these devices are prone to corrosion failure in atmospheric environments. To enhance conductivity and corrosion resistance, silver plating is applied to the contact surface of high-voltage switches. Common methods include graphite-Ag (G-Ag) coating, graphene-Ag (Gr-Ag) coating, and Ag-Sn coating. In this article, the corrosion resistance performance of silver plating, G-Ag coating, Gr-Ag coating, and Ag-Sn coating was studied. Firstly, adhesion tests were conducted on the plating layers. Subsequently, immersion experiments were performed to evaluate the corrosion resistance of the samples. Scanning electron microscopy (SEM), energy-dispersive X-ray spectroscopy (EDS), and laser confocal microscopy were used to analyze the morphology and elemental composition of the samples. Raman spectroscopy was used to analyze corrosion products. An electrochemical workstation was employed to study the electrochemical behavior of the samples. The adhesion results indicate that the adhesion of the plating layers is excellent. The immersion and electrochemical results showed the corrosion resistance order of the four Ag coatings was Ag-Sn coating > Gr-Ag coating > Ag coating > G-Ag coating.

**Keywords:** silver plating; graphene; corrosion resistance; high-voltage switch



**Citation:** Yang, B.; Chen, Y.; Hao, W.; Han, Y.; Zhang, Q.; Li, Y.; Wang, X.; Huang, L.; Lu, Y. The Corrosion Behavior of Different Silver Plating Layers as Electrical Contact Materials in Sulfur-Containing Environments.

*Coatings* **2023**, *13*, 1796. <https://doi.org/10.3390/coatings13101796>

Academic Editor: Peter Rodič

Received: 14 September 2023

Revised: 15 October 2023

Accepted: 16 October 2023

Published: 20 October 2023



**Copyright:** © 2023 by the authors. Licensee MDPI, Basel, Switzerland. This article is an open access article distributed under the terms and conditions of the Creative Commons Attribution (CC BY) license (<https://creativecommons.org/licenses/by/4.0/>).

## 1. Introduction

Electrical contact materials serve as conductive materials between electrical contact components, and their performance directly determines the reliability of electrical and electronic engineering. In the industry of high-voltage equipment, electrical contact materials are widely used in electrical equipment of power systems and are essential material components for outdoor high-voltage isolation switches [1,2]. A contact material mainly consists of a copper substrate and silver plating layer on the surface in domestic applications. Silver possesses excellent electrical and thermal conductivity, as well as corrosion resistance. However, silver has high costs when used. Copper, on the other hand, has strong conductivity and abundant reserves. However, copper has relatively high activity and tends to develop poor conductivity for the oxide layers on the surface, which can affect subsequent usage. The use of silver plating on copper substrates can improve their conductivity and corrosion resistance, thereby resolving cost-related issues [3–6].

During service, Cu-Ag contact material is continuously exposed to the atmospheric environment. When the contact surface is subjected to excessive relative humidity, a thin liquid film is generated on the surface, which constitutes an environment conducive to corrosion. Subsequently, the significant presence of a large number of corrosion products further increases the contact resistance of the switch [7], resulting in the occurrence of thermal defects during the operational lifespan of the switch [8–10]. During the operational

lifespan of contact materials, the soft nature of the silver plating layer makes it highly susceptible to wear and results in the exposure of the copper. A miniature galvanic cell is formed between the substrate and the plating layer in the ambient environment. Within this galvanic cell, copper acts as an anode and undergoes rapid consumption [11–13], which leads to an accelerated deterioration of the contact material [14].

To solve the failure problem of the contact material, the wear resistance and corrosion resistance of the silver plating layer should be improved. The surface treatment measures for high-voltage isolation switch contacts, both domestically and internationally, mainly include coating with conductive paste, adding corrosion-resistant coating [15–20], hard silver plating, and graphite silver plating. To enhance the longevity of the Ag coating on high-voltage isolating switch contact materials, the silver–graphite composite electroplating process has gradually become widely utilized for surface improvement treatment on the contact areas of isolating switches. Compared with pure silver coating, the advantages of both high electrical and thermal conductivity were exhibited in silver–graphite composite coatings, along with the lubricity and high hardness of graphite [4,5,21]. However, due to the continuous increase in the capacity of high-voltage isolation switches, the load per unit area of the contacts also sharply increases, which puts forward stricter requirements for the electrical contact performance of the contacts. The composite of silver and graphite has difficulty meeting the requirements of practical usage conditions.

Graphene, which is composed of a monolayer of carbon atoms densely packed into a two-dimensional hexagonal lattice structure, boasts a thickness of 0.35 nm in its single-layer form [22]. Graphene possesses excellent comprehensive performance. Its Young's modulus exceeds 1100 GPa [23]. Its thermal conductivity reaches up to 5000 W·m/K [24]. Its electron mobility at room temperature can reach as high as  $2 \times 10^5$  cm/V·s [25]. And its theoretical surface area is 2630 m<sup>2</sup>/g [26]. Graphene has been extensively used for its incorporation into graphene-reinforced metal matrix composites (GRMMCs), encompassing high-strength materials [27,28], conductive materials [29,30], thermal materials [31,32], and corrosion-resistant materials [33,34].

The existing research has made the graphene–silver coating a viable option. Kuang et al. [31] incorporated water-dispersible graphene oxide with excellent dispersion in a nickel plating bath containing aminosulfonic acid. Using electrodeposition techniques, the co-deposition of graphene with nickel was successfully achieved, and partial graphene in the coating was observed. Chen et al. [35] used a dual-pulse electrodeposition technique to fabricate composite coatings, and the incorporation of graphene resulted in a more compact surface morphology of the coatings. Pei et al. [36] found that the hardness of Ag-graphene coatings was significantly improved compared with pure Ag coatings. The graphene content in the plating solution was 10 g/L. Moreover, the corrosion resistance of Ag-graphene composite coatings was enhanced compared with pure Ag coatings. Wang et al. [37] discovered that the addition of graphene in silver coatings resulted in limited improvement of carbon content when the content of graphene increased. This limitation, in turn, hindered further enhancement of corrosion resistance. However, when the graphene content was 2 g/L, increasing the concentration of graphite in the plating solution significantly improved the overall performance of the composite coating. When the concentration of graphite was 30 g/L, the composite coating presented the best performance. Based on these findings, the silver/graphene composite coating has the potential to serve as a novel silver-based electrical contact material for upgrading outdoor high-voltage switch contact materials.

The addition of sulfur-resistant metallic elements to silver coatings can also enhance the corrosion resistance in sulfur-containing environments. In the early stages of exploration, the incorporation of precious metals was often required to achieve the high corrosion resistance in silver coatings [38]. However, it has been discovered that the addition of elements such as aluminum, copper, iron, and zinc to the coating can also improve the corrosion resistance of silver coatings in sulfur-containing environments [39]. The corrosion resistance of silver coatings in sulfur-containing environments can be significantly enhanced through alloying treatments. Sn has abundant natural resources, and its addition to silver coatings can greatly improve the

hardness of the coating while also reducing the cost of plating. According to the findings of Henry Leidheiser et al. [40], Ag-Sn coatings exhibit significantly good corrosion resistance in sulfur-containing environments. Similarly, Cai et al. [41] observed that electrodeposited Ag-Sn alloy coatings possess uniformity, density, and smoothness characteristics. Wang et al. [42] discovered that silver–tin alloy coatings possess superior corrosion resistance to graphene–silver coatings. Silver–tin alloy coatings exhibit excellent corrosion resistance, thermal conductivity, and wear resistance. They are currently widely used on the surfaces of high-voltage switches in various environments. However, the corrosion behavior of Ag coating, G coating, Gr coating, and Ag-Sn coating was unknown in sulfur-containing environments. This research can provide the basis for the choice of a silver coating.

In this study, to investigate the effect of different Ag coatings on the corrosion resistance of copper substrate, four coatings of the same thickness (Ag coating, G-Ag, Gr-Ag, Ag-Sn coating) were plated on the surface of the same copper substrate and subjected to an immersion experiment to accelerate the simulation of materials in the atmospheric environment service process. The corrosion rate, corrosion products, corrosion morphology, and other data were analyzed and compared to explore the corrosion resistance of the four coatings, providing theoretical reference for subsequent practical applications.

## 2. Experimental Methods

### 2.1. Sample Preparation

The four Ag coatings were obtained using an electroplating technique. Some of them have been used in electrical contact materials. Purple copper with the size of 70 mm × 20 mm × 2 mm was used as the experimental substrate. The samples were treated as follows in this experiment: degreasing → grinding → ultrasonic cleaning → alkali washing → water rinsing → acid washing → water rinsing → electroplating → water rinsing → hot water rinsing → drying. A silver graphite coating, Gr-Ag coating, and silver–tin alloy coating were prepared with a thickness of  $28 \pm 1 \mu\text{m}$  on the copper substrate (Figure 1). Four types of samples were cut into the size of 10 mm × 10 mm × 2 mm for electrochemical testing and the size of 40 mm × 20 mm × 2 mm for immersion testing. After being cut, the samples were cleaned with alcohol, dried, and weighed before the experiment.

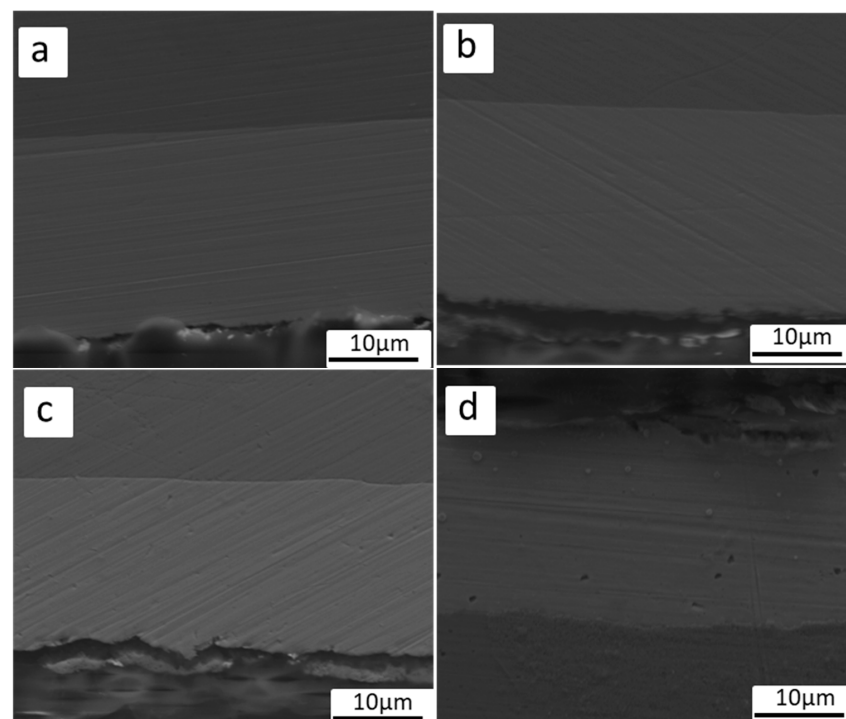


**Figure 1.** The cross-section morphology of four types of coatings: (a) Ag coating, (b) G-Ag coating, (c) Gr coating, (d) Ag-Sn coating.

## 2.2. Adhesion Test

The adhesion strength of the coatings was tested according to the GB/T 5270-2005 standard [43] of Test Methods for Adhesion Strength of Metallic Coatings on Metallic Substrates. The scratch method is as follows: Parallel lines on the surface were created using a scribe with a sharpening edge of  $30^\circ$  with a uniform streak. The distance between the lines was approximately 1 mm, and a square with a side length of 1 mm was forcibly scratched. The scribe marks should penetrate to the copper substrate. If the coating did not detach, it indicated good adhesion.

## 2.3. Immersion Experiment

Four coating samples were immersed in a 1 w%  $\text{Na}_2\text{S}$  solution to simulate the actual service environment. Three of the samples were used for weightlessness to reduce the error. One was used to analyze the corrosion products. The macro morphology was recorded using a camera during the immersion tests of 168 h.

### 2.3.1. Corrosion Morphology and Corrosion Product Analysis

The cross-section morphology of four coating samples was assessed using scanning electron microscopy (SEM) (FEI Quanta 200 F, Hillsboro, OR, USA). Additionally, the elemental composition variations within the coating area were analyzed by linear scans using energy-dispersive X-ray spectrometry (EDS). The macro morphology was recorded using a camera after immersion for 0 h, 12 h, 24 h, 72 h, 120 h, and 168 h. The corrosion morphology was observed using a laser confocal microscope (OLS4100, Tokyo, Japan) after 168 h of immersion. The type of corrosion products on the sample surface were analyzed using a laser Raman spectrometer (inVia Qontor, London, UK). Raman spectra were recorded with the 532 nm line of  $\text{Ar}^+$  laser excitation, using an inVia-Reflex micro-Raman system with a spectral resolution of  $2\text{ cm}^{-1}$ .

### 2.3.2. Weight Loss Test

After the immersion test, corrosion products were removed to obtain the corrosion rate using the weight loss method. The rust cleaning solution was a solution of 500 mL concentrated hydrochloric acid + 500 mL water + 3.5 g hexamethylenetetramine. The corrosion products on the surface of the sample were removed using the above solution in ultrasonic vibration. When the corrosion products were removed, the samples were taken out immediately. After pickling, the samples were rinsed multiple times with deionized water and dried. Finally, the dried samples were weighed again using an electronic balance with an accuracy of 0.1 mg.

## 2.4. Electrochemical Test

The electrochemical experiments (CHI660E, Shanghai, China) included open circuit potential (OCP), electrochemical impedance spectroscopy (EIS), and polarization curve tests. The electrochemical test was conducted using a three-electrode system, with a saturated calomel electrode (SCE) as the reference electrode, a platinum electrode as the auxiliary electrode (CE), and different silver-plated samples (with an exposed area of  $1\text{ cm}^2$ ) as the working electrode (WE). The electrochemical test solution was a 1 w%  $\text{Na}_2\text{S}$  solution. During the electrochemical test, the open circuit potential measurement was performed first. After stabilization, the EIS measurement was conducted using a frequency range of  $10^5\text{ Hz}$  to  $10^{-2}\text{ Hz}$  and an amplitude of 10 mV. The polarization curve test was conducted with a cathodic potential range of  $-200\text{ mV}$  (vs. OCP). The anodic test was terminated when the pitting potential was reached. The scan rate was set at  $0.5\text{ mV/s}$ . Each electrochemical test was repeated at least three times until the repeatability was good. After the experiment, the EIS data were analyzed and fitted using ZSimpWin 3.60 software. The corrosion potential and other parameters of the polarization curve were fitted using Origin software 2018.

All tests were carried out at room temperature.

### 3. Results

#### 3.1. The Adhesion of the Coating and the Composition of the Coating

To observe the degree of adhesion between the coating and substrate, the adhesion of the coating was tested according to the GB/T 5270-2005 standard [43]. The scratch test was performed using the grid method as shown in Figure 2. None of the four types of coatings exhibited blistering or coating detachment. From the reference of GB/T 9286-2021 [44], the adhesion levels can be divided into levels of 0 to 5. When the edge is completely smooth and there is no loss in the grid, it can be classified as level 0. So, in this adhesion test, the adhesion levels of the four coating samples were rated as 0.

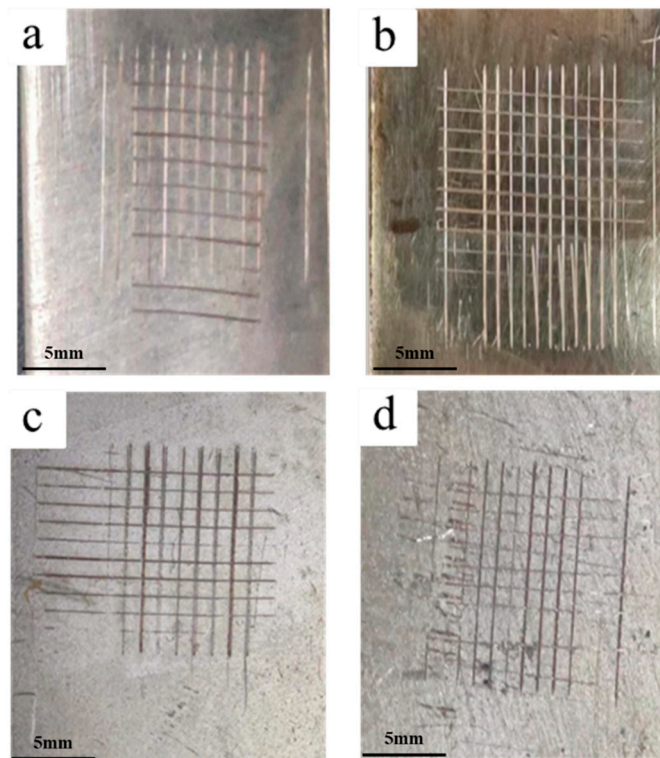


**Figure 2.** Adhesion strength testing of four coatings: (a) Ag coating, (b) G-Ag coating, (c) Gr-Ag coating, (d) Ag-Sn coating.

Figure 3 shows the cross-section microstructure images and the EDS analysis of the four types of coatings. The cross-section microstructure images show that the Ag-Sn coating bonds well with Cu and there are some defects between the Ag, G-Ag, and Gr-Ag coatings and Cu matrix, which indicates the Ag-Sn coating has a good combination with Cu. The composition of the interface was analyzed using the line scanning of EDS. As shown in Figure 3a, elemental analysis of silver coating was performed. Cu was observed in the substrate, while Ag was detected within the coating. Ag was found exclusively in the coating and dominated the main composition. No substrate elements were found in the coating, and the coating and substrate had a distinct separation. Figure 3b represents the elements of the G-Ag coating. It was mainly composed of Ag and C. The Cu from the substrate was not found in the coating, and the distribution of Ag and C in the coating was relatively uniform. Figure 3c represents the Gr-Ag coating, which was primarily composed of Ag. No traces of Cu were found in the coating, and both Ag and C were evenly distributed within the coating. Figure 3d depicts a Ag-Sn coating. It was primarily composed of Ag and Sn. No Cu appeared in the coating. The boundary between the coating and the substrate was clearly defined. It was observed that a lower concentration of Sn and a higher concentration of Ag existed close to the side of the substrate in the coating. The concentration of Sn increased away from the substrate and eventually dominated the coating.

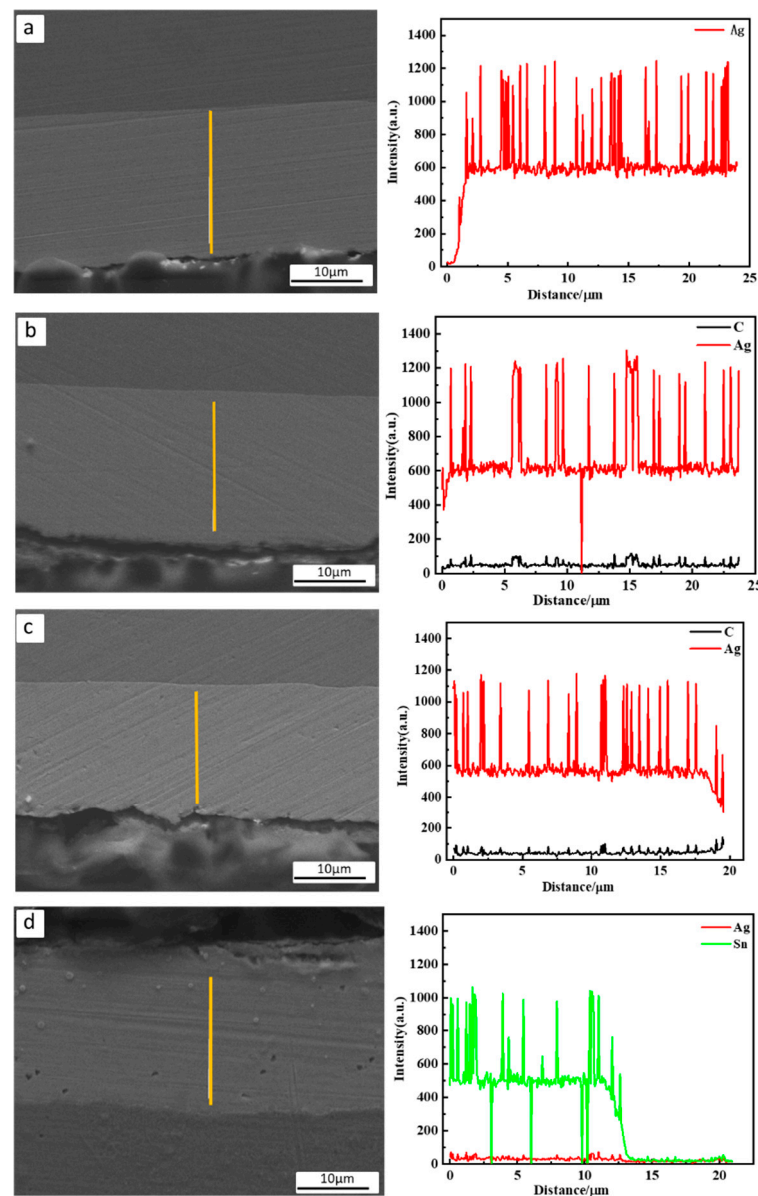


**Figure 3.** The cross-section microstructure image as determined by SEM and composition of film as determined by EDS for the four coating samples: (a) Ag coating, (b) G-Ag coating, (c) Gr-Ag coating, (d) Ag-Sn coating.

### 3.2. Corrosion Morphology Characteristics

The macroscopic morphology of the four types of coatings with different immersion times is shown in Figure 4. From the macroscopic images, it was evident that the corrosion degree of the silver-plated samples gradually intensified with the increase in immersion time. However, the corrosion morphology showed a significant difference. During the immersion process, a layer of yellow-brown corrosion product appeared on the surface of the silver coating. As time elapsed, multiple corrosion pits developed on the surface, and the thickness of the corrosion product gradually increased. A layer of yellow-brown corrosion product formed in the G-Ag coating during the immersion process. There was also a noticeable tendency for color change in the corrosion product. The Gr-Ag coating formed a thin layer of yellow-brown corrosion product during immersion. As time increased, this layer of corrosion product gradually thickened. The Ag-Sn coating exhibited the mildest corrosion among the different coatings. The color of the surface gradually changed from its original bright white color to yellow. With immersion time

prolonged, corrosion products also appeared on the surface of the coating. Compared with the macro morphology of the four coatings, it was observed that the G-Ag coating had the highest amount of corrosion products and suffered from the most severe corrosion. This may be due to the galvanic corrosion that may occur between graphite and Ag. Ag was the anode and graphite was the cathode, and Ag exhibited accelerated corrosion. On the other hand, the Ag-Sn coating had the fewest corrosion products and exhibited good corrosion resistance.

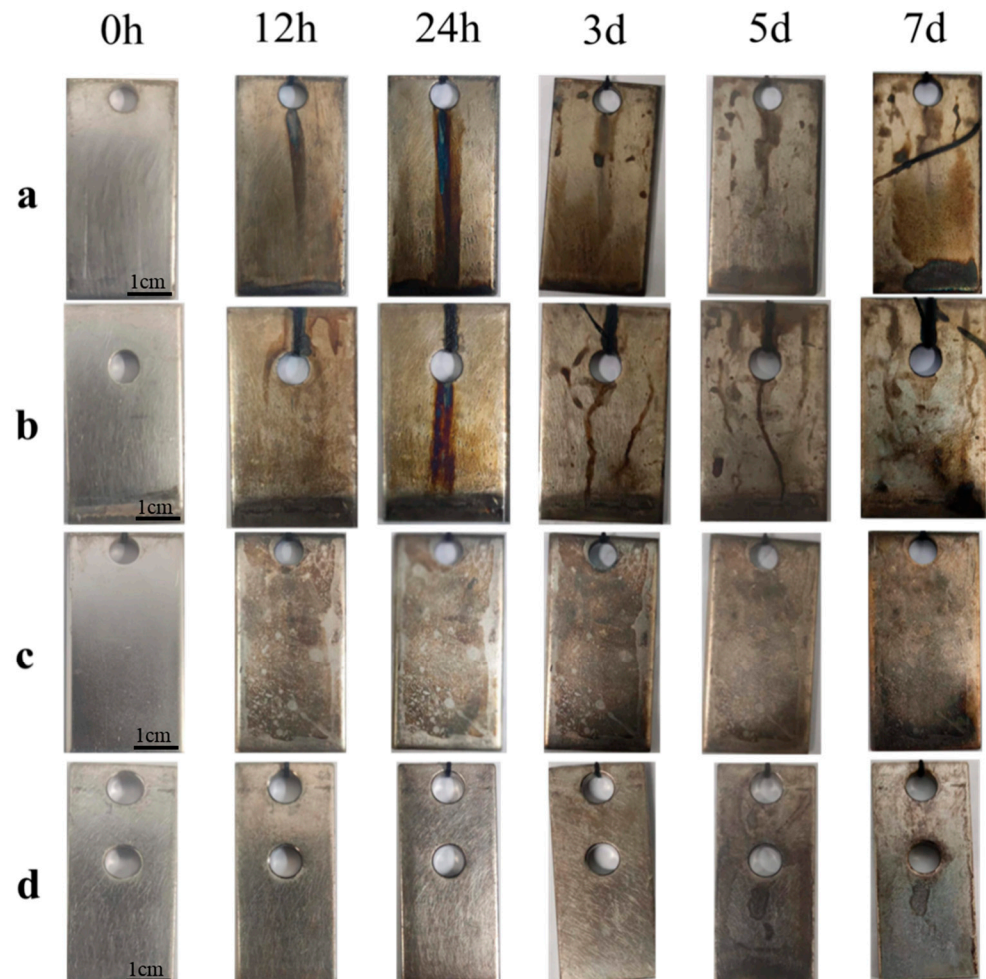


**Figure 4.** The macroscopic corrosion morphology after immersion in 1 w%  $\text{Na}_2\text{S}$  solution for 168 h: (a) Ag coating, (b) G-Ag coating, (c) Gr-Ag coating, (d) Ag-Sn coating. All the pictures are on the same scale.

To further observe the corrosion morphology of the coatings after immersion, laser confocal microscopy was utilized to observe the samples with rust and the samples after the removal of the corrosion products (Figure 5). The pitting depth is indicated by the variation in the color. The deeper the color change, the larger the pits. Figure 5(a<sub>1</sub>,a<sub>2</sub>) shows the localized microscopic morphology of the silver coating. After immersion for 168 h, a partial accumulation of corrosion products appeared on the surface, and the scratches became shallower. Some pits also emerged. After corrosion products were removed, a greater number of pits were observed, as demonstrated in Figure 5(a<sub>3</sub>,a<sub>4</sub>). Through statistical analysis, the maximum depth of pits was determined to be 11.811  $\mu\text{m}$ . Figure 5(b<sub>1</sub>,b<sub>2</sub>) illustrates the localized microscopic morphology of the G-Ag coating. After 168 h of immersion, a significant amount of corrosion products appeared on the sample surface. The predominant form of corrosion was uniform corrosion, but a few pits were still observed. After the corrosion products were removed, the G-Ag coating surface exhibited

a uniform distribution of flake graphite, as shown in Figure 5(b<sub>3</sub>,b<sub>4</sub>). The depth of the pits was relatively small, and the maximum depth was about 10.139  $\mu\text{m}$ . Figure 5(c<sub>1</sub>,c<sub>2</sub>) depicts the localized microscopic morphology of the Gr-Ag coating. After 168 h of immersion, the sample surface was covered with corrosion products. Similar to the other samples, the corrosion form was mainly uniform corrosion with a lesser number of pits. After the corrosion products were removed, the sample surface exhibited a uniform distribution of stable graphene particles, as shown in Figure 5(c<sub>3</sub>,c<sub>4</sub>). The maximum depth of pits was only 5.091  $\mu\text{m}$ , which was lower than that of the other samples. This could be attributed to the uniform distribution of graphene within the silver coating. Figure 5(d<sub>1</sub>,d<sub>2</sub>) depicts the localized microscopic morphology of the Ag-Sn coating surface. After 168 h of immersion, the scratches on the sample surface became shallower. The surface of the sample was covered with some corrosion products, and a few pits were present. The corrosion was primarily localized corrosion. After the corrosion products were removed, the coating surface exhibited numerous pits with different depths, as shown in Figure 5(d<sub>3</sub>,d<sub>4</sub>). The maximum depth of pits on the coating surface was about 6.665  $\mu\text{m}$ . Compared with the microscopic morphologies of the four coatings in a sulfur-containing environment, it could be observed that the Ag-Sn coating showed the least corrosion, followed by the Gr-Ag coating, while the silver-plated coating showed the poorest corrosion resistance.

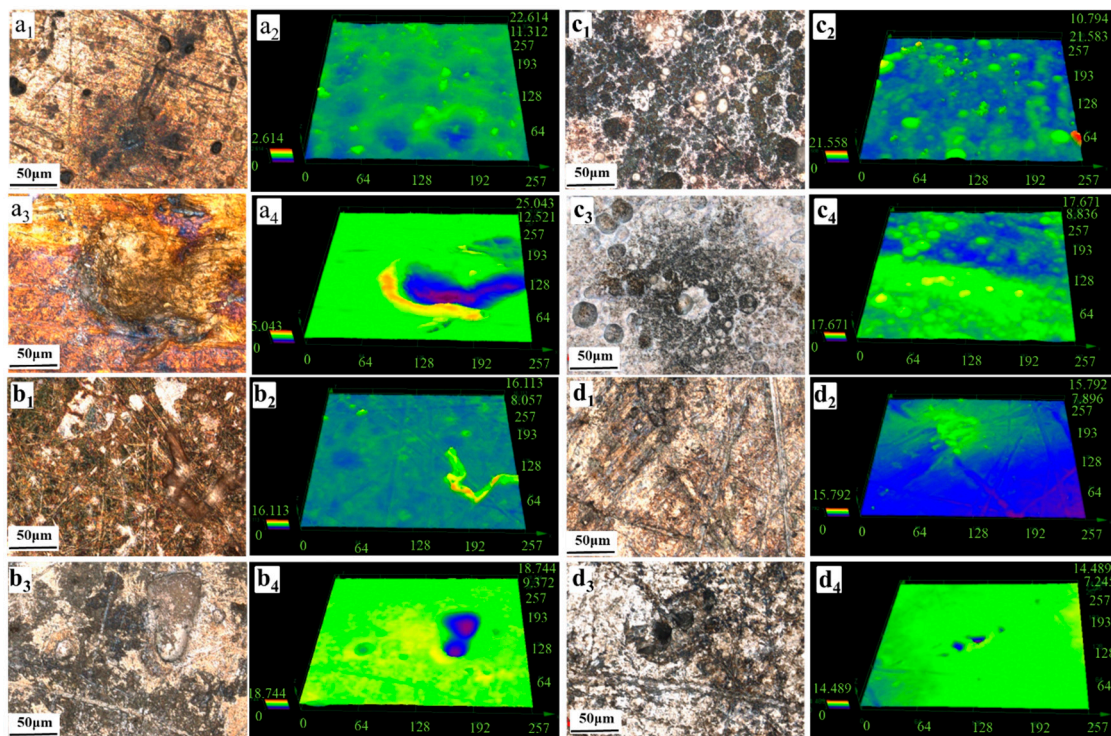


**Figure 5.** Laser confocal morphology after 168 h of immersion: (a) Ag coating, (b) G-Ag coating, (c) Gr-Ag coating, and (d) Ag-Sn coating.

### 3.3. Corrosion Product Analysis

Raman testing was conducted on the G-Ag coating and the Gr-Ag coating before immersion corrosion. From Figure 6a, it can be observed that characteristic peaks of carbon were detected in both the G-Ag and Gr-Ag coatings. This indicated that graphite and graphene are uniformly dispersed within the coatings. The characteristic peaks of graphene were found at the same position as the characteristic peaks of graphite, but the ID/IG ratio of graphene was smaller. Figure 6b presents the Raman spectroscopy analysis of the corrosion products after 168 h of corrosion in a sulfur-containing environment for the four coatings. The main compounds identified were  $\text{Ag}_2\text{S}$  and  $\text{Ag}_2\text{O}$ . The corrosion products of the silver coating primarily consisted of  $\text{Ag}_2\text{S}$  and  $\text{Ag}_2\text{O}$ . The corrosion products of the

G-Ag and Gr-Ag coatings were mainly composed of silver sulfide, with a small amount of  $\text{Ag}_2\text{O}$ . The corrosion products of the Ag-Sn coating contained  $\text{Ag}_2\text{O}$ ,  $\text{Ag}_2\text{S}$ , and  $\text{SnS}$  simultaneously. The types of corrosion products were similar among the four coatings. The silver coatings exhibited evident oxidation and hydrogen evolution corrosion in the sulfur-containing environment.

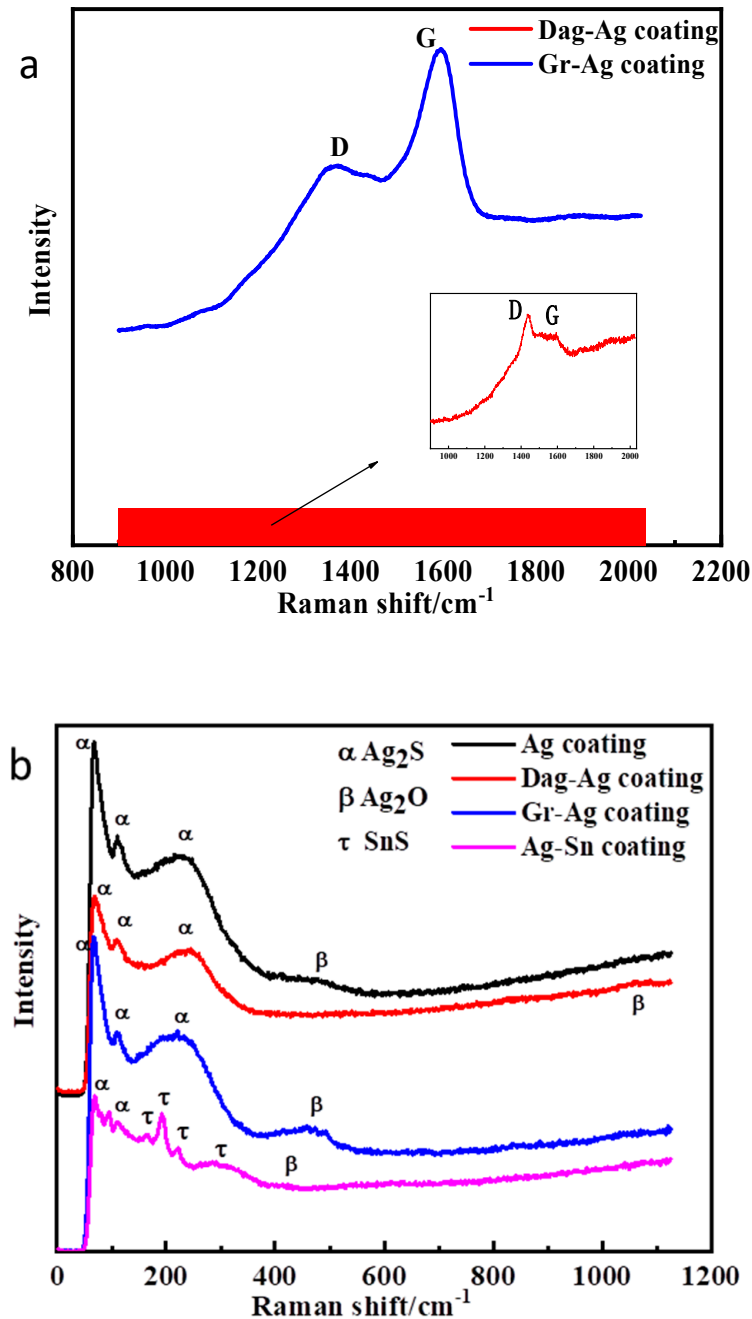


**Figure 6.** (a) Raman peaks of G-Ag and Gr-Ag coatings; (b) Raman peaks of corrosion products of the four coatings after immersion.

### 3.4. Corrosion Rate Analysis

Figure 7 displays the corrosion rates of the four coatings after immersion in a 1 w%  $\text{Na}_2\text{S}$  solution for 168 h. It can be clearly observed that the corrosion rates of the Ag coating, G-Ag coating, Gr-Ag coating, and Ag-Sn coating were 0.2876 mm/a, 0.5322 mm/a, 0.2372 mm/a, and 0.1557 mm/a, respectively. Based on the corrosion rate values, it can be

seen that the corrosion rates of the four coating specimens in a 1 w%  $\text{Na}_2\text{S}$  solution were as follows: G-Ag coating > Ag coating > Gr-Ag coating > Ag-Sn coating.

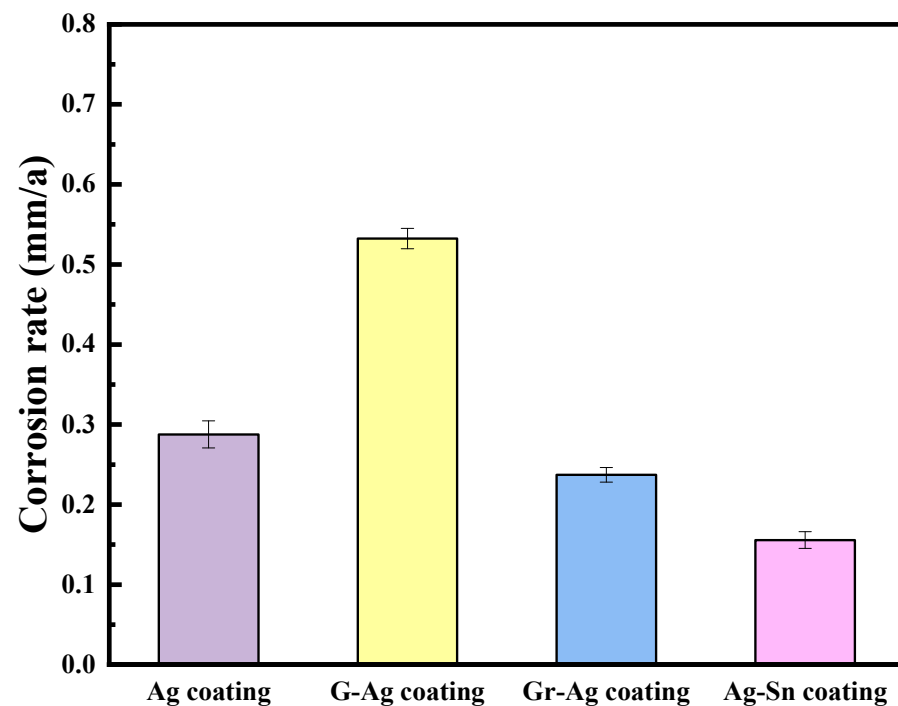


**Figure 7.** The corrosion rates of four different silver-plated layers during a 168 h testing period.

### 3.5. Electrochemical Measurement Analysis

The corrosion behavior of four silver-coated samples in a sulfur-containing environment was analyzed through an electrochemical test. Figure 8a shows the Nyquist diagram and Figure 8b shows the Bode mode value diagram and phase angle diagram of the four silver-plated samples. The Nyquist diagram shows that the arc radius of the Ag-Sn coating is significantly higher than that of the other three coating samples, and the arc radius of the G-Ag coating is the smallest. This shows that the Ag-Sn coating has the best corrosion resistance, and the G-Ag coating has the worst corrosion resistance.

To better analyze the electrochemical behavior of the four coating patterns, impedance fitting analysis was carried out. From the phase angle diagram, it can be found that the Ag-Sn coating has two platforms and the Ag, G-Ag, and Gr-Ag coatings have at least three platforms, which explains the interface changing differently. In the Nyquist diagram, the low-frequency area was in the fourth quadrant for the Ag, G-Ag, and Gr-Ag coatings, which indicates there may be some corrosion products in the surface generating the dispersion effects of corrosion products. So, there were two capacitive reactances in Ag-Sn coating and two capacitive resistances and one inductive resistance in the three other coatings. The fitting circuit is shown in Figure 9, and the fitting results are shown in Table 1. Here,  $R_s$  is a solution resistor,  $Q_f$  is a surface film constant-phase-angle element,  $R_f$  is a film resistor,  $R_{ct}$  is a charge transfer resistor,  $Q_d$  is a double electric layer constant-phase-angle element, and  $L$  is an inductor element. In Table 1, it can be seen that the charge-transfer resistance values of the four coating samples are Ag coating:  $171.1 \Omega \cdot \text{cm}^2$ , G-Ag coating:  $159 \Omega \cdot \text{cm}^2$ , Gr-Ag coating:  $318 \Omega \cdot \text{cm}^2$ , and Ag-Sn coating:  $3128 \Omega \cdot \text{cm}^2$ . The charge transfer resistance of the Ag-Sn coating is the highest, which indicates that the resistance is larger and the corrosion resistance is better. On the contrary, the charge transfer resistance of the G-Ag coating is the smallest, which indicates that the resistance is the smallest and the corrosion resistance is low. This may be because the graphite particles in the G-Ag coating are large, and the dispersion of graphite is not very good in the coating. The graphene particle size is small, and graphene is well dispersed in the silver plating layer, reflecting better corrosion resistance.

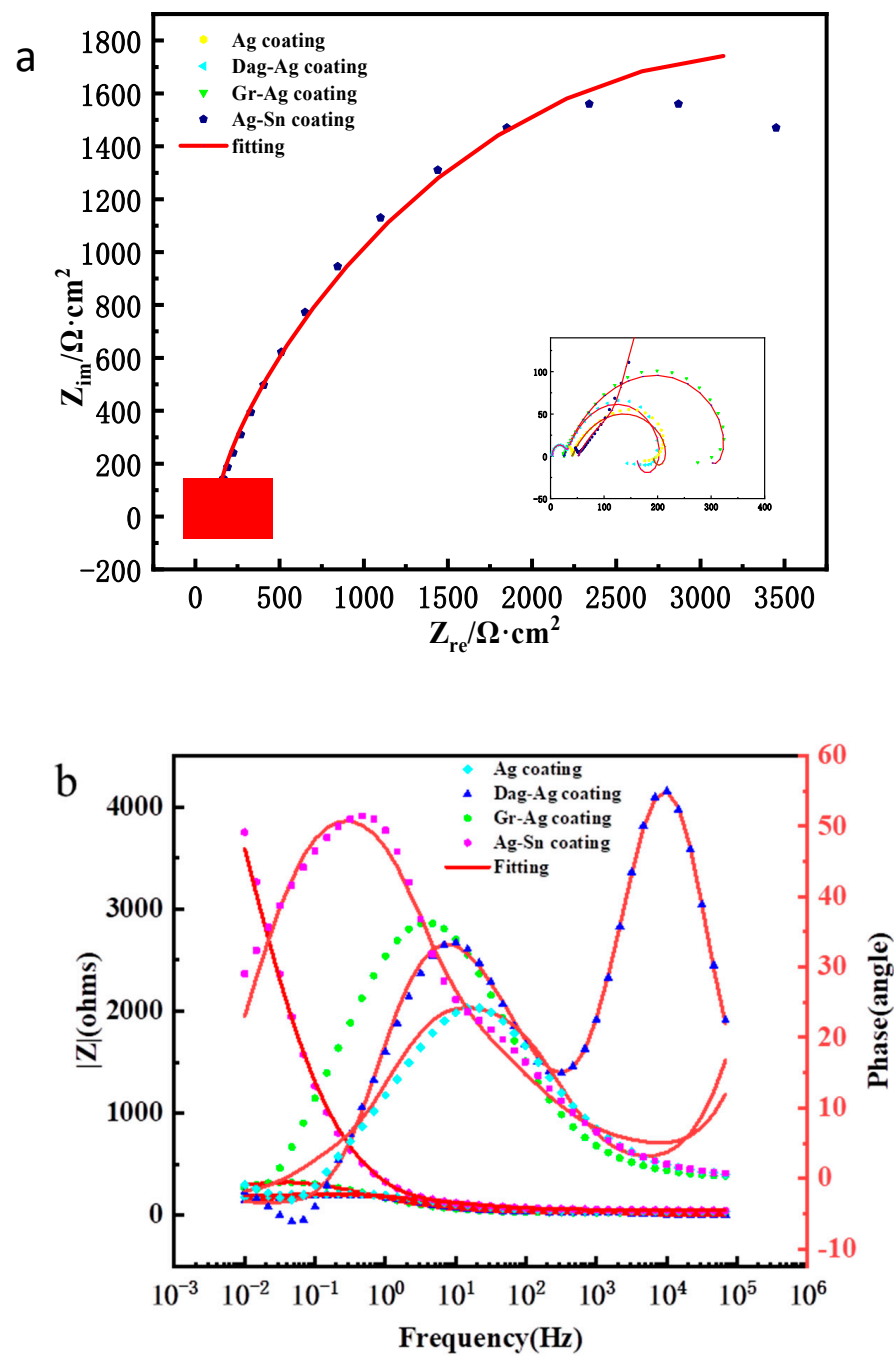


Figure 8. Nyquist (a) and Bode (b) diagrams of the four coatings in 1 w% Na<sub>2</sub>S solution.

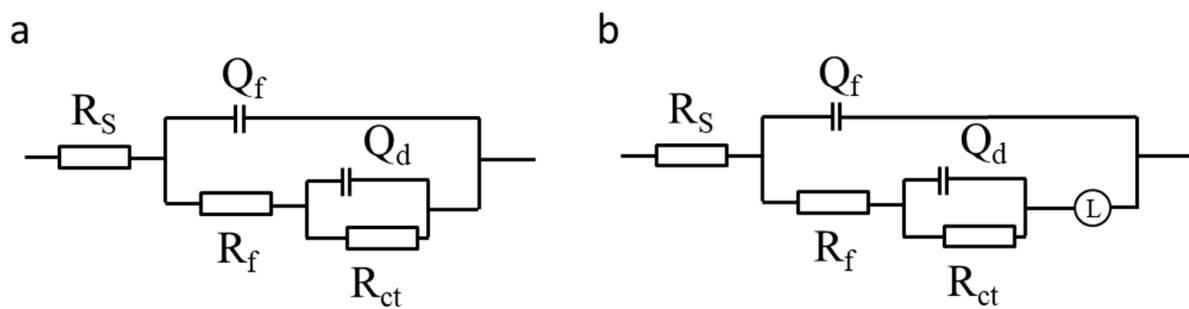
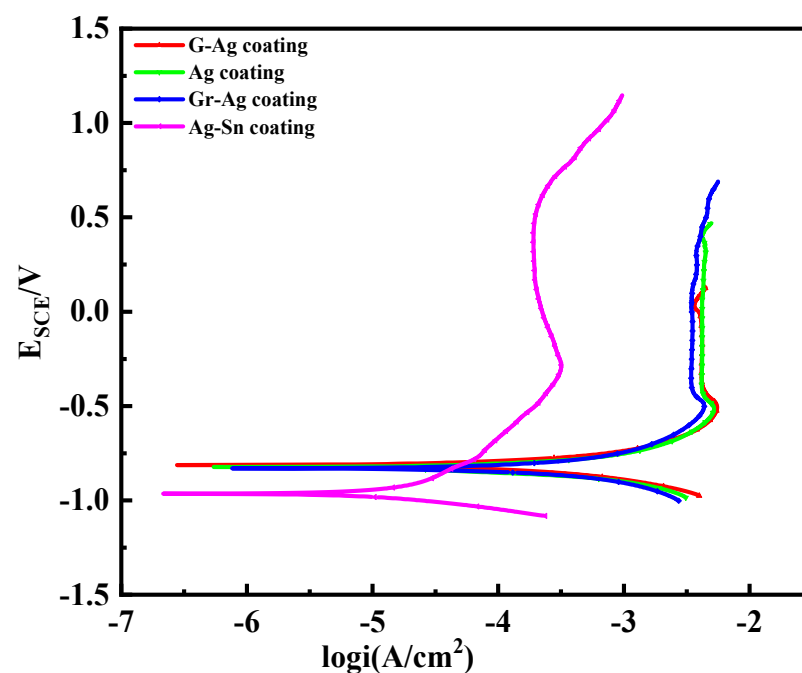


Figure 9. Fitted circuits of the four coatings in 1 w% Na<sub>2</sub>S solution: (a) silver coating, (b) other coatings.

**Table 1.** Impedance curve fitting data of four silver-plated samples.

Type	$R_s$ ( $\Omega \cdot \text{cm}^2$ )	$Q_f$ ( $\text{mF} \cdot \text{cm}^2$ )	$R_f$ ( $\Omega \cdot \text{cm}^2$ )	$Q_d$ ( $\text{mF} \cdot \text{cm}^2$ )	$R_{ct}$ ( $\Omega \cdot \text{cm}^2$ )	$L$ ( $\Omega \cdot \text{cm}^2$ )
Ag	18.22	$8.394 \times 10^{-6}$	22.88	$5.243 \times 10^{-4}$	171.1	$1.568 \times 10^{-5}$
G-Ag	39.77	$2.156 \times 10^{-6}$	26.56	$7.149 \times 10^{-4}$	159	$1.569 \times 10^{-5}$
Gr-Ag	0.56	$1.374 \times 10^{-6}$	24.69	$1.306 \times 10^{-3}$	318.7	$5.527 \times 10^4$
Ag-Sn	2.484	$2.089 \times 10^{-6}$	30.96	$1.157 \times 10^{-3}$	3128	

The polarization curves of the four coating samples in the  $\text{Na}_2\text{S}$  solution are shown in Figure 10. It can be seen from the shape of the polarization curve that the overall polarization curve of the Ag-Sn coating was close to the leftmost, while the polarization curves of the G coating, Ag coating, and Gr-Ag coating were relatively close to the right. This indicates that the Ag-Sn coating sample has better corrosion resistance than the other three samples. The corrosion potential and corrosion current of the four samples were calculated using the Tafel extrapolation method, as shown in Table 2. The results show that the corrosion potential of the Ag-Sn coating is more negative, and the corrosion tendency is the largest, but the corrosion rate is the smallest, only  $5.24 \times 10^{-5} \text{ A/cm}^2$ . The corrosion tendencies of the other three coatings are similar, and their corrosion potentials are similar. The corrosion potentials are  $-0.823 \text{ V}$  (Ag coating),  $-0.812 \text{ V}$  (G-Ag coating), and  $-0.830 \text{ V}$  (Gr-Ag coating). The corrosion tendency of these three coatings is lower than that of the Ag-Sn coating. However, the corrosion current density of the three coatings is higher than that of the Ag-Sn coating. The corrosion current densities from high to low are as follows: G-Ag coating ( $1.38 \times 10^{-3} \text{ A/cm}^2$ ), Ag coating ( $1.23 \times 10^{-3} \text{ A/cm}^2$ ), and Gr-Ag coating ( $1.17 \times 10^{-3} \text{ A/cm}^2$ ). This means that the corrosion rate of the Ag-Sn coating in the  $\text{Na}_2\text{S}$  environment is lower than that of the other three coatings. When the polarization potential further increases, the passivation phenomenon can be found in all four kinds of coatings in the  $\text{Na}_2\text{S}$  solution, and the pitting potential and passivation interval are shown in Table 2. The Gr-Ag coating has the highest pitting potential and the widest dimensional passivity region, while the G-Ag coating has the lowest pitting potential. From the perspective of dimensional passivation potential range, the four coatings have good passivation stability. The pitting potential order of the four coatings in a 1 wt%  $\text{Na}_2\text{S}$  solution is as follows: Gr-Ag coating > Ag-Sn coating > Ag coating > G-Ag coating.

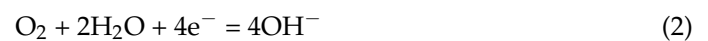
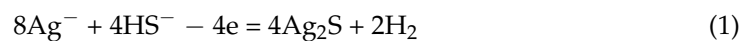
**Figure 10.** Polarization curves of the four coatings in 1 wt%  $\text{Na}_2\text{S}$  solution.

**Table 2.** Polarization curve fitting data of four silver-plated samples.

Type	$E_{\text{corr}}/\text{V}$	$I_{\text{corr}}/\text{A}\cdot\text{cm}^{-2}$	$E_p/\text{V}$	Passivation Region
Ag	−0.823	$1.23 \times 10^{-3}$	0.403	−0.409 V~0.377 V
G-Ag	−0.812	$1.38 \times 10^{-3}$	0.036	−0.369 V~−0.006 V
Gr-Ag	−0.830	$1.17 \times 10^{-3}$	0.599	−0.395 V~0.584 V
Ag-Sn	−0.964	$5.24 \times 10^{-5}$	0.594	−0.267~0.594 V

#### 4. Discussion

The main problem faced by copper-based silver-plated electrical contact materials during service in atmospheric environments is the corrosion of the surface silver (Ag) plating by trace amounts of sulfides. In moist atmospheric environments, a thin liquid film can easily form on the surface of the Ag coating, which can facilitate the ionization of sulfides into  $\text{HS}^-$  ions. These  $\text{HS}^-$  ions then react with Ag and lead to the formation of sulfides on the surface of the plating [45–48]. The reaction process is as follows:



When a thin liquid film is formed on the Ag surface, the first reaction is prone to occur. Then, black sulfides are formed on the surface of the plating. Simultaneously, when Ag in the plating is oxidized, it combines with the  $\text{OH}^-$  generated in reaction 2 to form AgOH. But AgOH is highly unstable and readily decomposes into stable  $\text{Ag}_2\text{O}$ . The reaction process is as follows:



Raman data showed that the types of corrosion products of the four coatings were roughly the same. The reaction occurred in a  $\text{Na}_2\text{S}$  solution, and a layer of black sulfide was formed. Carbon has good reducibility and can effectively inhibit the oxidation of Ag; thus, the formation of sulfide slowed down. Sn exists in the Ag-Sn coating, and the reducing property of Sn is weak, which cannot effectively hinder the oxidation of Ag. In a  $\text{Na}_2\text{S}$  solution, Ag and Sn react together and form the corresponding sulfide. Sn and Ag are uniformly mixed in the Ag Sn coating, and the density of Ag and Sn is similar to that of the pure silver coating. The Ag-Sn coating is relatively dense on the Cu matrix, which isolates the contact between the coating and the solution more or less. As a result, the intensity and quantity of the characteristic peaks of  $\text{Ag}_2\text{S}$  corrosion products on the Ag-Sn coating are less than those of the other three coatings.

Similar conclusions can be obtained from the electrochemical data. According to the AC impedance and polarization curves, the capacitive loop of the Ag-Sn coating is the largest, while that of the G-Ag coating is the smallest (Figure 8). Except for Ag-Sn coating, the low frequency appeared in the fourth quadrant, which means inductive reactance may exist. This may be due to the layer of corrosion products, which makes ion migration difficult. In the polarization curve test, the corrosion current density of the Ag-Sn sample was the smallest ( $5.24 \times 10^{-5} \text{ A/cm}^2$ ), while the corrosion current density of the G-Ag coating was the largest ( $1.38 \times 10^{-3} \text{ A/cm}^2$ ), as shown in Table 2. This is consistent with the results of Lv et al. [49]. They mentioned that the corrosion resistance of Gr-Ag coating samples is higher than that of Ag coating samples. Due to the large particle size of graphite, the coating is loose, and the specific surface area is larger, so the sodium sulfide solution has more contact with the coating, and more corrosion products are produced on the surface. On the contrary, the particle size of graphene is small, and graphene has a special structure. The addition of graphene not only does not affect the density of the

coating but also improves the corrosion resistance of the Ag coating. So, the corrosion resistance of the Gr-Ag coating is better than that of the Ag coating and G Ag coating. As for the Ag-Sn coating, Sn is added to the coating, and Sn and Ag are oxidized in a Na<sub>2</sub>S solution to produce the corresponding sulfide (Figure 6b); the reaction between Sn and HS<sup>-</sup> is dominant in the immersion process due to the stronger reduction of Sn than Ag. In addition, the sulfide of Sn is more stable than that of Ag<sub>2</sub>S and can form a physical barrier on the surface of the coating and prevent the coating from continuing to react with HS<sup>-</sup>. As a result, the corrosion resistance of the Ag-Sn coating in the Na<sub>2</sub>S system is higher than that of the Gr-Ag coating. The results of electrochemical corrosion resistance are consistent with those of corrosion rate, which has the same result. The corrosion rate order is as follows: G-Ag > Ag coating > Gr coating > Ag-Sn coating. So, the Gr-Ag coating and Sn-Ag coating can be used as electrical contact materials for outdoor high-voltage switches.

All these results were obtained in a laboratory experiment; more data can be obtained from research in real-world conditions. This may be a limitation of this study, and researchers should study Ag coatings in real-world conditions in the future. The Gr-Ag coating and Sn-Ag coating may be studied to determine the reason for their good corrosion resistance.

## 5. Conclusions

1. The Ag coating, G coating, Gr coating, and Ag-Sn coating studied have good bonding force, as determined in an adhesion test, and this illustrates that the electroplating technique is good.
2. Ag, Sn, and graphite had good dispersibility in the four coatings, as shown by the cross-section morphology. After the immersion test, the corrosion products on the surface of the four coatings had silver sulfide and silver oxide, as shown by Raman analysis.
3. Through the electrochemical and immersion tests, statistically, it was found that the corrosion resistance of the four coating samples was sorted as follows: the corrosion resistance of the Ag-Sn coating was higher than that of the Gr-Ag coating, which was higher than that of the Ag coating, and the G-Ag coating had the worst corrosion resistance. The Gr-Ag coating and Sn-Ag coating are better choices than the Ag coating.

**Author Contributions:** Conceptualization and methodology, B.Y. and Y.C.; validation, B.Y., W.H. and Y.H.; formal analysis, B.Y.; investigation, B.Y., Q.Z. and Y.L. (Yujie Li); resources, B.Y.; data curation, B.Y. and X.W.; writing—original draft preparation, B.Y.; writing—review and editing, B.Y., Q.Z. and L.H.; supervision, B.Y., Y.C. and Y.L. (Yiliang Lu). All authors have read and agreed to the published version of the manuscript.

**Funding:** This work is supported by the project from headquarters science and technology of State Grid Corporation of China (No. 5500-202158364A-0-0-00).

**Institutional Review Board Statement:** Not applicable.

**Informed Consent Statement:** Not applicable.

**Data Availability Statement:** All the data included in this article are available upon request by contact the corresponding author.

**Conflicts of Interest:** The authors declare no conflict of interest.

## References

1. Grandin, M.; Wiklund, U. Friction, wear and tribofilm formation on electrical contact materials in reciprocating sliding against silver-graphite. *Wear* **2013**, *302*, 1481–1491. [[CrossRef](#)]
2. Qiyang, T.; Xiaolong, Z.; Yunhong, Z. Electrical contact properties of AgCuO electrical contact materials. *Chin. J. Nonferrous Met.* **2015**, *25*, 1244–1249.
3. Kun, Y.; Gao, S.; Dexin, C.; Yanmiao, H.; Fantian, L. Experimental Study on Contact Life of Disconnecting Switch. *Smart Grid* **2014**, *2*, 63–66.

4. Kim, B.G.; Choi, S.K.; Chung, H.S.; Lee, J.J.; Saito, F. Grinding characteristics of crystalline graphite in a low-pressure attrition system. *Powder Technol.* **2002**, *126*, 22–27. [[CrossRef](#)]
5. Liu, N.; Qi, S.; Li, S.; Wu, X.; Wu, L. Preparation and characterization of phenol formaldehyde/Ag/graphite nanosheet composites. *Polym. Test* **2011**, *30*, 390–396. [[CrossRef](#)]
6. Marx, D.E.; Barillo, D.J. Silver in medicine: The basic science. *Burns* **2014**, *40*, S9–S18. [[CrossRef](#)]
7. Zhao, C.; Wang, X.; Yu, B.; Cai, M.; Yu, Q.; Zhou, F. Research Progress on the Wear and Corrosion Resistant Plasma Electrolytic Oxidation Composite Coatings on Magnesium and Its Alloys. *Coatings* **2023**, *13*, 1189. [[CrossRef](#)]
8. Jiyue, Z.; Zhenglai, S.; Gongcun, W.; Xinggang, Z.; Zhengyong, X.; Fei, X. Reason Analysis and Measures for Contact Heat of GW4 Isolating Switch. *J. Anhui Electr. Eng. Vocat. Tech. Coll.* **2014**, *19*, 16–19.
9. Yongjun, X.; Cheng, X.; Yijun, Z.; Lizhong, J.; Zhangjie, C. Development and Application of Live Contact Resistance Measurement Unit of Disconnecter. *Zhejiang Electr. Power* **2016**, *35*, 25–27.
10. Fuyong, W.; Huagui, C. Heat Analysis of Outdoor Isolator Contacts Considering Thermal Field. *High Volt. Appar.* **2011**, *47*, 81–86.
11. Nazarov, A.P.; Thierry, D. Probing of Atmospheric Corrosion of Metals: Carbon Steel. *Prot. Met.* **2004**, *40*, 377–388. [[CrossRef](#)]
12. Rudolphi, A.K.; Bjorkman, C.; Imrell, T.; Jacobson, S. Conduction through corrosion films on silver plated copper in power contacts. In Proceedings of the Electrical Contacts—1995, Proceedings of the Forty-First IEEE Holm Conference on Electrical Contacts, Montreal, QC, Canada, 2–4 October 1995; pp. 124–134.
13. Mikhailov, A.A. Effect of low-molecular carbon acids on atmospheric corrosion of metals. *Prot. Met. Phys. Chem. Surf.* **2009**, *45*, 757–765. [[CrossRef](#)]
14. Keqin, Z. Study on the Corrosion Behavior of the Switch Contactmaterial under the Electric Current and the Ag-Grapheneanti-Corrosion Coating. Master's Thesis, South China University of Technology, Guangzhou, China, 2019.
15. Verma, C.; Thakur, A.; Ganjoo, R.; Sharma, S.; Assad, H.; Kumar, A.; Quraishi, M.A.; Alfantazi, A. Coordination bonding and corrosion inhibition potential of nitrogen-rich heterocycles: Azoles and triazines as specific examples. *Coord. Chem. Rev.* **2023**, *488*, 215177. [[CrossRef](#)]
16. Thakur, A.; Kaya, S.; Kumar, A. Recent Innovations in Nano Container-Based Self-Healing Coatings in the Construction Industry. *Curr. Nanosci.* **2022**, *18*, 203–216. [[CrossRef](#)]
17. Thakur, A.; Kumar, A.; Kaya, S.; Marzouki, R.; Zhang, F.; Guo, L. Recent Advancements in Surface Modification, Characterization and Functionalization for Enhancing the Biocompatibility and Corrosion Resistance of Biomedical Implants. *Coatings* **2022**, *12*, 1459. [[CrossRef](#)]
18. Daoudi, W.; El Aatiaoui, A.; Dagdag, O.; Zaidi, K.; Haldhar, R.; Kim, S.-C.; Oussaid, A.; Aouinti, A.; Berisha, A.; Benhiba, F.; et al. Anti-Corrosion Coating Formation by a Biopolymeric Extract of Artemisia herba-alba Plant: Experimental and Theoretical Investigations. *Coatings* **2023**, *13*, 611. [[CrossRef](#)]
19. Thakur, A.; Kaya, S.; Kumar, A. Recent Trends in the Characterization and Application Progress of Nano-Modified Coatings in Corrosion Mitigation of Metals and Alloys. *Appl. Sci.* **2023**, *13*, 730. [[CrossRef](#)]
20. Muresan, L.M. Nanocomposite Coatings for Anti-Corrosion Properties of Metallic Substrates. *Materials* **2023**, *16*, 5092. [[CrossRef](#)]
21. Rong, M.Z. The recent advances in electrical contact and arc research. *Electr. Eng.* **2005**, *05*, 1363–1376.
22. Cheng, X.C.; Zhou, Y.; Jiang, Z.X.; Dai, W.; Liu, X.Y.; Zhai, S.Y. Study on graphene oxide in the function of drug delivery and biosafety. *Biomed. Eng. Clin. Med.* **2012**, *16*, 402–405.
23. Lee, C.; Wei, X.; Kysar, J.W.; Hone, J. Measurement of the Elastic Properties and Intrinsic Strength of Monolayer Graphene. *Science* **2008**, *321*, 385–388. [[CrossRef](#)] [[PubMed](#)]
24. Balandin, A.A.; Ghosh, S.; Bao, W.; Calizo, I.; Teweldebrhan, D.; Miao, F.; Lau, C.N. Superior Thermal Conductivity of Single-Layer Graphene. *Nano Lett.* **2008**, *8*, 902–907. [[CrossRef](#)] [[PubMed](#)]
25. Bolotin, K.I.; Sikes, K.; Jiang, Z.; Klima, M.; Fudenberg, G.; Hone, J.; Kim, P.; Stormer, H.L. Ultrahigh electron mobility in suspended graphene. *Solid State Commun.* **2008**, *146*, 351–355. [[CrossRef](#)]
26. Zhang, Y.B.; Tan, Y.W.; Stormer, H.L.; Kim, P. Experimental Observation of Quantum Hall Effect and Berry's Phase in Graphene. *Nature* **2005**, *438*, 201–204. [[CrossRef](#)]
27. Dixit, S.; Mahata, A.; Mahapatra, D.R.; Kailas, S.V. Multi-layer graphene reinforced aluminum—Manufacturing of high strength composite by friction stir alloying. *Compos. Part B Eng.* **2018**, *136*, 63–71. [[CrossRef](#)]
28. Du, X.; Du, W.B.; Wang, Z.H.; Liu, K.; Li, S.B. Ultra-high strengthening efficiency of graphene nanoplatelets reinforced magnesium matrix composites. *Mater. Sci. Eng. C* **2018**, *711*, 633–642. [[CrossRef](#)]
29. Khobragade, N.; Kumar, B.; Bera, S.; Roy, D. Studies on graphene reinforced Cu base composites prepared by two step thermal processing method. *Mater. Today Proc.* **2017**, *4*, 8045–8051. [[CrossRef](#)]
30. Xie, G.; Forslund, M.; Pan, J. Direct Electrochemical Synthesis of Reduced Graphene Oxide (rGO)/Copper Composite Films and Their Electrical/Electroactive Properties. *ACS Appl. Mater. Interfaces* **2014**, *6*, 7444–7455. [[CrossRef](#)]
31. Kuang, D.; Xu, L.; Liu, L.; Hu, W.; Wu, Y. Graphene–nickel composites. *Appl. Surf. Sci.* **2013**, *273*, 484–490. [[CrossRef](#)]
32. Wejrzanowski, T.; Grybczuk, M.; Chmielewski, M.; Pietrzak, K.; Kurzydowski, K.J.; Strojny-Nedza, A.J.M. Thermal conductivity of metal-graphene composites. *Mater. Design* **2016**, *99*, 163–173. [[CrossRef](#)]
33. Kumar, C.M.; Venkatesha, T.V.; Shabadi, R. Preparation and corrosion behavior of Ni and Ni-graphene composite coatings. *Mater. Res. Bull.* **2013**, *48*, 1477–1483. [[CrossRef](#)]

34. Prasai, D.; Tuberquia, J.C.; Harl, R.R.; Jennings, G.K.; Bolotin, K.I. Graphene: Corrosion-inhibiting coating. *ACS Nano* **2012**, *6*, 1102–1108. [[CrossRef](#)] [[PubMed](#)]
35. Chen, J.; Li, J.; Xiong, D.; He, Y.; Ji, Y.; Qin, Y. Preparation and tribological behavior of Ni-graphene composite coating under room temperature. *Appl. Surf. Sci.* **2016**, *361*, 49–56. [[CrossRef](#)]
36. Pei, F.; Zhou, Y.; Tian, X.; Liu, X.; Ye, Z.G. Study on Preparation and Properties of Silver-Graphene Coating for Outdoor Isolating Switch. *Mater. Prot.* **2022**, *55*, 87–92.
37. Jiancai, W.; Feng, P.; Xu, T.; Guang, M.; Loulu, J.; Zhiguo, Y. Preparation and Properties of Electrical Contact Silver/Graphite/Graphene Composite Coatings for Outdoor High-voltage Disconnectors. *Mod. Chem. Res.* **2022**, *20*, 14–16.
38. Menghua, M. A Non-rusting silver-alloy and its preparation. *China Molybdenum Ind.* **2003**, *1*, 44–45.
39. Wang, Y.F.; Chen, F.Y.; Liu, Z.P.; Du, S.Y.; Ying, J.M. Effects of graphene content on the microstructure and properties of copper matrix composites. *Carbon* **2016**, *96*, 836–842.
40. Leidheiser, H.; Ghuman, A.R.P. Pulse Electroplating of Silver-Tin Alloys and the Formation of Ag<sub>3</sub>Sn. *J. Electrochem. Soc.* **1973**, *120*, 484–487. [[CrossRef](#)]
41. Jiqing, C. Electroplating Sn-Ag alloy. *Corros. Prot.* **2000**, *5*, 214–215.
42. Wang, X.Y.; Xue, J.H.; Xie, M.F.; Wang, Z.H.; Qiao, X.Y. Electrodeposition Preparation and Comparison of Antitarnish Properties of Four Kinds of Coatings. *Plating Finish.* **2020**, *42*, 12–16.
43. GB/T 5270-2005; Metallic Coatings on Metallic Substrates—Electrodeposited and Chemically Deposited Coatings—Review of Methods Available for Testing Adhesion. State Administration for Market Regulation: Beijing, China, 2005.
44. GB/T 9286-2021; Paints and Varnishes—Cross-Cut Test. State Administration for Market Regulation: Beijing, China, 2021.
45. Graedel, T.E. Corrosion Mechanisms for Silver Exposed to the Atmosphere. *J. Electrochem. Soc.* **1992**, *139*, 1963. [[CrossRef](#)]
46. Thakur, A.; Kumar, A.; Sharma, S.; Ganjoo, R.; Assad, H. Computational and experimental studies on the efficiency of *Sonchus arvensis* as green corrosion inhibitor for mild steel in 0.5 M HCl solution. *Mater. Today Proc.* **2022**, *66*, 609–621. [[CrossRef](#)]
47. Bashir, S.; Thakur, A.; Lgaz, H.; Chung, I.-M.; Kumar, A. Computational and experimental studies on Phenylephrine as anti-corrosion substance of mild steel in acidic medium. *J. Mol. Liq.* **2019**, *293*, 111539. [[CrossRef](#)]
48. Parveen, G.; Bashir, S.; Thakur, A.; Saha, S.K.; Banerjee, P.; Kumar, A. Experimental and computational studies of imidazolium based ionic liquid 1-methyl-3-propylimidazolium iodide on mild steel corrosion in acidic solution. *Mater. Res. Express.* **2019**, *7*, 016510. [[CrossRef](#)]
49. Wangyan, L.; Wenjun, W.; Ming, N.; Feng, H.; Yingchao, Y.; Keqin, Z.; Chaochao, Z. Green Preparation and Performance Optimization for Ag-graphene Composite Coatings for High-voltage Isolation Switch. *Guangdong Electr. Power* **2019**, *32*, 112–123.

**Disclaimer/Publisher’s Note:** The statements, opinions and data contained in all publications are solely those of the individual author(s) and contributor(s) and not of MDPI and/or the editor(s). MDPI and/or the editor(s) disclaim responsibility for any injury to people or property resulting from any ideas, methods, instructions or products referred to in the content.